1 Perturbative Stability of Massless Scalars in AdS_4

Having examined the collapse of massive scalars fields in AdS_5, we now wish to explore the perturbatively stable solutions for massless scalars. These solutions resist collapse on time scales of $t \sim \epsilon^{-2}$ and give analytic descriptions of the direct and inverse energy cascades that must be balanced for stability to be achieved.

Using the Two-Time Formalism (TTF), renormalization flow equations are derived that absorb secular terms into renormalized integration constants in the first-order solution for the scalar field. These flow equations can be combined using a quasi-periodic (QP) ansatz to relate the amplitude and phases and lead to a system of $j_{max}+1$ QP equations that relate the $j_{max}+3$ unknowns. While the TTF theory technically involves an infinite sum of terms, by truncating the series to a finite j_{max} value, numerical values for the amplitudes and phases can be calculated. How the truncation value affects the space of solutions, and the limits of the solution space itself, remains to be addressed.

1.1 Contributions of Authors

In this collaboration, QP solutions to (1.19) were found numerically through programs initially written by N. Deppe, but later expanded and developed by myself. In particular, I developed code to achieve the tail fitting and seeding procedure detailed in appendix 1.A that allowed for solutions to (1.19) to be developed for j_{max} values of several hundred – almost an order of magnitude greater than the solutions previous found in the literature. Implementation of the high temperature perturbation method outlined in 1.4.2 was done using code I developed, as was the procedure of reoptimization

that allowed for the high temperature solution to be projected back to the QP solution plane at various frequencies. Evolution of the solutions was based on numerical methods initially developed by N. Deppe. All data management and analysis was done using programs written by myself.

Much of the numerical work for this project was done using the University of Winnipeg's tesla server, where CPU hours are not tracked. However, for larger systems increased computing power was required, which necessitated transferring all code to Compute Canada's new Cedar cluster. Once there, I used 5.43 CPU years' worth of computing power to run evolutions and analysis of the results. Finally, I wrote the paper, with input from the other authors, that appears here.

As is common for these types of projects, all members of the collaboration were equally involved in the interpretation of the data, as well as the late stages of editing. Authors are listed alphabetically and it is understood that all members contribute equally to the publication.

On the Stability of High-Temperature, Quasi-Periodic Solutions for Massless Scalars in AdS_4

To Appear on arxiv.org

Brad Cownden[1], Nils Deppe[2], and Andrew R. Frey[3,4]

[1]*Department of Physics & Astronomy,*

University of Manitoba

Winnipeg, Manitoba R3T 2N2, Canada

cowndenb@myumanitoba.ca

[2]*Cornell Center for Astrophysics and Planetary Science and Department of Physics,*

Cornell University

122 Sciences Drive, Ithaca, New York 14853, USA

nd357@cornell.edu

[3]*Department of Physics & Astronomy,*

University of Manitoba

Winnipeg, Manitoba R3T 2N2, Canada

[4]*Department of Physics and Winnipeg Institute for Theoretical Physics,*

University of Winnipeg

515 Portage Avenue, Winnipeg, Manitoba R3B 2E9, Canada

a.frey@uwinnipeg

We construct a families of perturbative solutions for massless scalar fields in AdS_4 by solving the renormalization flow equations derived from the Two-Time Formalism using a quasi-periodic (QP) ansatz. We verify that these solutions are robust against the choice of truncation and examine their evolution within the perturbative framework. Furthermore, we investigate methods for extending the space of such solutions and find that the space of solutions is much more restricted than previously thought. In particular, several families of solutions that appear to solve the system at

low truncation number fail to do so as the truncation value is increased. We show that new families of QP solutions are accessible only through evolution of the perturbative system.

1.2 Introduction

The question of the nonperturbative stability of $(d+1)$-dimensional Anti-de Sitter spacetime has been examined extensively, both as a question of mathematical physics and given its application to the AdS/CFT correspondence (see reviews such as [?]). Beginning with the seminal work of [?], the generic instability of spherically symmetric AdS_{d+1} gravity minimally coupled to a scalar field has been repeatedly demonstrated [?, ?, ?, ?, ?]. The primary driver of the instability in the fully nonlinear system is the weakly turbulent flow of energy to short length scales. However, [?, ?, ?] (and others) have shown that some initial conditions in asymptotically AdS spacetimes resist gravitational collapse; these conditions form islands of stability in the space of initial data. As these islands of stability continue to be explored, more subtle behaviours have been identified, particularly along the "shorelines" [?, ?, ?, ?]. Within the stability islands are various solutions created from exciting a single linear mode, known as oscillons or breathers for real scalars [?, ?, ?, ?], boson stars for complex scalars (on a fixed metric) [?, ?], and geons in pure gravity [?, ?].

While the nonperturbative physics of AdS instability requires numerical study, the perturbative formulation encapsulates the weakly turbulent nonlinear physics at $\mathcal{O}(\epsilon^3)$. At this order, resonances can be removed at each order by frequency shifts; however, data constructed from superpositions of eigenmodes contain resonances that cannot be removed this way [?]. For fields constructed from multiple excited eigenmodes, the secular growth of resonant terms that satisfy certain frequency conditions triggers the onset of instability [?, ?, ?, ?].

To control the secular growth, the amplitude and phase of each eigenmode are allowed to flow with respect to a second scale. Applying renormalization techniques to these new slowly-varying amplitudes and phases leads to a ladder of coupled first-order ordinary differential equations describing the flow. There are several equivalent methods to arrive at the flow equations: the Two-Time

Formalism (TTF) – wherein the slow time $\tau = \epsilon^2 t$ is the flow parameter [?] – a renormalization-like formalism [?, ?], and time averaging procedure [?, ?]. By absorbing the secular terms into the renormalized amplitudes and phases, the $\mathcal{O}(\epsilon^3)$ resonances are controlled and collapse is avoided over time scales of $t \sim \epsilon^{-2}$.

In order to solve the flow equations for a general scalar field, one naturally has truncate the mode expansion at a maximum eigenmode number j_{max}. After having found solutions to the truncated TTF system, one can probe their stability by taking a quasi-periodic (QP) ansatz for the amplitude/phase variables. These QP solutions orbit static solutions in phase space, have constant energy E and particle number[1] N, and are categorized in terms of the "temperature" $T = E/N$ [?, ?]. Understanding the bounds of the space of QP solutions allows us to better understand how to construct more general long-lived scalar fields. QP solutions are special in that the time-dependence of each mode is harmonic, so QP solutions satisfy algebraic equations. The first families of solutions were classified as "low-temperature" and were found by directly solving these algebraic equations [?]. It was then suggested that the space of solutions could be extended into higher temperatures by perturbing low-temperature solutions, up to a maximum temperature of $T_{max} = 2j_{max} + d$.

In this work, we examine the persistence of QP solutions, especially those with high temperatures, in the limit of large j_{max} to eliminate the influence of truncation effects on the solutions. The space of high temperature solutions is explored using established perturbative methods and solutions are tested against various choices of j_{max}. The stability of both classes of solutions are examined through indicators such as the scalar curvature and energy transfer among eigenmodes.

This work is organized as follows: we begin in § 1.3 with a review of the linearized solutions for a minimally coupled, massless scalar field in AdS_{d+1} and establish the renormalization flow equations that govern the time evolution of the amplitude and phase functions in the scalar field. In § 1.4, we find quasi-periodic solutions in AdS_4 by directly solving a set of algebraic equations and establish the bounds of low-temperature QP solutions. We then consider methods of expanding the space of QP solutions to include high-temperature solutions in § 1.4.2. Evolution of all QP solutions in the

[1] The symmetries inherent to the TTF system yield these two conserved quantities [?].

perturbative theory is presented § 1.5. We end with a discussion of results § **??**.

1.3 Minimally Coupled Scalar Fields in AdS$_{d+1}$

Consider a spherically-symmetric, asymptotically AdS$_{d+1}$ spacetime with characteristic curvature $L = 1$. Written in Schwarzschild-like coordinates, the metric in units of AdS scale is given by

$$ds^2 = \frac{1}{\cos^2(x)}\left(-Ae^{-2\delta}dt^2 + A^{-1}dx^2 + \sin^2(x)d\Omega^{d-1}\right)\,, \tag{1.1}$$

where the radius $x \in [0, \pi/2]$ and $-\infty < t < \infty$. A minimally-coupled, massless scalar field $\phi(t, x)$ is subject to the following Einstein and Klein-Gordon equations:

$$G_{ab} + \Lambda g_{ab} = 8\pi\left(\nabla_a\phi\nabla_b\phi - \frac{1}{2}g_{ab}(\nabla\phi)^2\right) \tag{1.2}$$

$$0 = \frac{1}{\sqrt{-g}}\partial_a\sqrt{-g}\,g^{ab}\partial_b\phi\,. \tag{1.3}$$

The canonical equations of motion for the scalar field are

$$\partial_t\phi = Ae^{-\delta}\Pi, \quad \partial_t\Phi = \partial_x(Ae^{-\delta}\Pi), \quad \text{and} \quad \partial_t\Pi = \frac{\partial_x\left(\Phi Ae^{-\delta}\tan^{d-1}(x)\right)}{\tan^{d-1}(x)}\,, \tag{1.4}$$

where the canonical momentum is $\Pi(t, x) = A^{-1}e^{\delta}\phi$ and $\Phi(t, x) \equiv \partial_x\phi$ is an auxiliary variable. In terms of these fields, (1.2)-(1.3) reduce to

$$\partial_x\delta = -\left(\Pi^2 + \Phi^2\right)\sin(x)\cos(x), \tag{1.5}$$

$$\partial_x A = \frac{d - 2 + 2\sin^2(x)}{\sin(x)\cos(x)}(1 - A) - A\sin(x)\cos(x)(\Pi^2 + \Phi^2)\,. \tag{1.6}$$

1.3.1 Linearized Solutions

The linearized scalar field solutions come from expanding in terms of a small amplitude

$$\phi(t,x)=\sum_{j=0}^{\infty}\epsilon^{2j+1}\phi_{2j+1}(t,x),\quad A(t,x)=1-\sum_{j=1}^{\infty}\epsilon^{2j}A_{2j}(t,x),\quad \delta(t,x)=\sum_{j=1}^{\infty}\epsilon^{2j}\delta_{2j}(t,x). \tag{1.7}$$

Under this expansion, the $\mathcal{O}(\epsilon)$ terms give the linearized equation of motion for the scalar field:

$$\partial_t^2\phi_1+\hat{L}\phi_1=0\quad\text{where}\quad \hat{L}_1\equiv-\frac{1}{\tan^{d-1}(x)}\partial_x\left(\tan^{d-1}(x)\partial_x\right)\,. \tag{1.8}$$

The eigenvalues of $\hat{L}$ are simply $\omega_j^2=(d+2j)^2$ and the eigenfunctions are

$$e_j(x)=k_j\cos^d(x)P_j^{(\frac{d}{2}-1,\frac{d}{2})}\left(\cos(2x)\right)\quad\text{with}\quad k_j=\frac{2\sqrt{j!(j+d-1)!}}{\Gamma(j+\frac{d}{2})}\,. \tag{1.9}$$

Note the the normalizations are chosen such that $\hat{L}e_j=\omega_j^2e_j$ and

$$\langle e_i|e_j\rangle\equiv\int_0^{\frac{\pi}{2}}dx\,\bar{e}_ie_j\tan^{d-1}(x)\,. \tag{1.10}$$

By expanding the scalar field functions in terms of the eigenbasis given in (1.9) and substituting into (1.8), we find that the time-dependent functions $c_n^{(2j+1)}(t)=\langle\phi_{2j+1}(t,x),e_n(x)\rangle$ satisfy $\ddot{c}_j^{(1)}+\omega_j^2c_j^{(1)}=0$. The general solution for the scalar field is can then be written in terms of time-dependent amplitude and phase variables:

$$\phi_1(t,x)=\sum_{j=0}^{\infty}A_j(t)\cos\left(\omega_jt+B_j(t)\right)e_j(x)\,. \tag{1.11}$$

As discussed in [?, ?, ?], the integer nature of the mode frequencies mean that the spectrum is fully resonant. Unlike solutions such as oscillons, the resonant terms cannot be absorbed by a frequency shift and therefore result in *secular* terms: resonant contributions that grow rapidly with time and induce collapse. These resonant terms appear at $\mathcal{O}(\epsilon^3)$ and can be expressed in terms of a source,

$S(t)$:

$$\ddot{\phi}_3 + \hat{L}\phi_3 = S \equiv 2(A_2 - \delta_2)\ddot{\phi}_1 + (\dot{A}_2 - \dot{\delta}_2)\dot{\phi}_1 + (A_2' - \delta_2')\phi_1' \,, \tag{1.12}$$

where A_2, δ_2 are the leading-order contributions to the metric functions in (1.7) that are determined by the $\mathcal{O}(\epsilon^2)$ backreaction with the metric. Projecting onto the $e_j(x)$ basis, the source term can be expressed in terms of the time-dependent coefficients

$$\ddot{c}_j^{(3)} + \omega_j^2 c_j^{(3)} = S_j \,. \tag{1.13}$$

To control the growth of secular terms, [**?**] used resummation techniques to absorb singular contributions into the amplitude A_j and phase B_j of (1.11). This also resulted in a set of conserved quantities: the energy of the system, E, and particle number, N. The simultaneous conservation of both E and N imply the existence of inverse energy cascades that must balance direct cascades, and provide a mechanism through which two-mode data could remain stable [**?**].

1.3.2 Two-Time Formalism

The Two-Time Formalism (TTF) describes the solution to (1.8) in terms of slowly-modulating amplitude and phase variables, A_j and B_j, that are functions of the slow time $\tau = \epsilon^2 t$,

$$\phi(t, x) = \epsilon \sum_{j=0}^{\infty} A_j(\epsilon^2 t) \cos\left(\omega_j t + B_j(\epsilon^2 t)\right) e_j(x). \tag{1.14}$$

The next non-trivial order in the equations of motion include gravitational self-interactions of the scalar field, and provides source terms for A_j and B_j. Following the time-averaging procedure of [**?**] – and using the resonance condition $\omega_i + \omega_j = \omega_k + \omega_\ell$ to eliminate one of the indices – the ℓ^{th}

amplitude and phase are given by

$$-\frac{2\omega_\ell}{\epsilon^2}\frac{dA_\ell}{dt} = \sum_{i\neq\ell}^{\ell\leq i+j}\sum_{j\neq\ell} S_{ij(i+j-\ell)\ell}A_iA_jA_{i+j-\ell}\sin\left(B_\ell + B_{i+j-\ell} - B_i - B_j\right), \tag{1.15}$$

$$\begin{aligned}-\frac{2\omega_\ell A_\ell}{\epsilon^2}\frac{dB_\ell}{dt} &= T_\ell A_\ell^3 + \sum_{i\neq\ell} R_{i\ell}A_i^2A_\ell \\ &\quad + \sum_{i\neq\ell}^{\ell\leq i+j}\sum_{j\neq\ell} S_{ij(i+j-\ell)\ell}A_iA_jA_{i+j-\ell}\cos\left(B_\ell + B_{i+j-\ell} - B_i - B_j\right).\end{aligned} \tag{1.16}$$

The coefficients T, R, S are calculated directly from integrals over the product of eigenmodes and contain some useful symmetry properties: the integrals vanish except with the resonance condition $\omega_i + \omega_j = \omega_\ell$ is met.

Computationally, we find it more convenient to write T, R, S in terms of auxiliary coefficients with greater symmetry properties (as shown in [**?**]). The explicit expressions for these integrals in the interior gauge, in which $\delta(t, x = 0) = 0$, are given in appendix 1.B.

Using a complex amplitude of the form $\mathcal{A}_j(\tau) = A_j\exp(-iB_j)$ in (1.14) allows us to combine equations (1.15) and (1.16) into a single TTF equation:

$$-2i\omega_\ell\frac{\mathcal{A}_\ell}{d\tau} = T_\ell|\mathcal{A}_\ell|^2\mathcal{A}_\ell + \sum_{i\neq\ell} R_{i\ell}|\mathcal{A}_i|^2\mathcal{A}_\ell + \sum_{i\neq\ell}^{\ell\leq i+j}\sum_{j\neq\ell} S_{ij(i+j-\ell)\ell}\mathcal{A}_i\mathcal{A}_j\bar{\mathcal{A}}_{i+j-\ell}\,. \tag{1.17}$$

1.4 Quasi-periodic Solutions in AdS_4

The stability of the solutions to (1.17) can be examined using a *quasi-periodic* (QP) ansatz for the complex amplitude,

$$\mathcal{A}_j = \alpha_j e^{i\beta_j\tau}\,, \tag{1.18}$$

where $\alpha_j, \beta_j \in \mathbb{R}$. Substituting (1.18) into (1.14) allows us to relate the QP modes α_j and β_j to the amplitude/phase modes via $A_j = 2\alpha_j$, $B_j = \beta_j\tau$. When we examine how well the QP solutions

solve the Einstein equations, we use this conversion to re-construct the scalar and metric fields from the QP solutions. The time dependence in (1.17) is removed via the condition $\beta_j = \beta_0 + j(\beta_1 - \beta_0)$, leaving β_0 and β_1 as unknown parameters. Considering modes of (1.14) up to some j_{max}, the QP ansatz results in a set of $j_{max}+1$ algebraic equations for $j_{max}+3$ unknowns

$$2\omega_\ell \alpha_\ell \beta_\ell = T_\ell \alpha_\ell^3 + \sum_{i\neq\ell} R_{i\ell}\alpha_i^2\alpha_\ell + \sum_{i\neq\ell}^{\ell\leq i+j}\sum_{j\neq\ell} S_{ij(i+j-\ell)\ell}\alpha_i\alpha_j\alpha_{i+j-\ell}\,. \tag{1.19}$$

As shown in [**?**, **?**], the TTF is invariant under a $U(1)$ transformation that leads to the conserved quantities

$$E = 4\sum_j \omega_j^2\alpha_j^2 \qquad \text{and} \qquad N = 4\sum_j \omega_j\alpha_j^2\,. \tag{1.20}$$

These definitions allow for two of the free parameters to be fixed. Families of solutions can be examined by fixing $\alpha_0 = 1$ and sampling a range of α_1 values in the range $\alpha_1 \ll \alpha_0$. The families of solutions can be distinguished by their "temperature", or energy per particle number $T = E/N$.

Practically speaking, finding solutions to the j_{max} equations that arise from (1.17) requires truncating the series at a finite value $j_{max} < \infty$. However, solutions must continue to be present and unaffected by increasing j_{max} to represent true solutions to the TTF theory.

1.4.1 Persistence at Large j_{max}

The question of edge effects in determining the stability of a particular solution is important to investigate. For instance, if a particular solution to (1.19) is found for some α_1 when $j_{max} = 50$, does this continue to be a solution when we consider more modes, say $j_{max} = 250$? By following the methods outlined in appendix 1.A, we are able to start with a low j_{max} solution and incrementally increase the number of modes being considered up to several hundred. This method was found to be more successful, given the optimization algorithms being used, than other seeding methods.

As an example, consider solutions to (1.19) with the conditions $\alpha_0 = 1.0$ (since all QP solutions

are defined up to an overall scale, $\alpha_0 = 1.0$ is taken to always be true) and $\alpha_1 = 0.2$, which corresponds to an initial temperature of $T_0 \simeq 3.146$. In figure 1.1a, we present an overlay of QP solutions generated by successive solving, fitting, and seeding from $j_{max} = 50$ to $j_{max} = 500$ for a family of QP solutions. Similar high j_{max} solutions were confirmed for $\alpha_1 \leq 0.442$ and are shown in figure 1.1b.

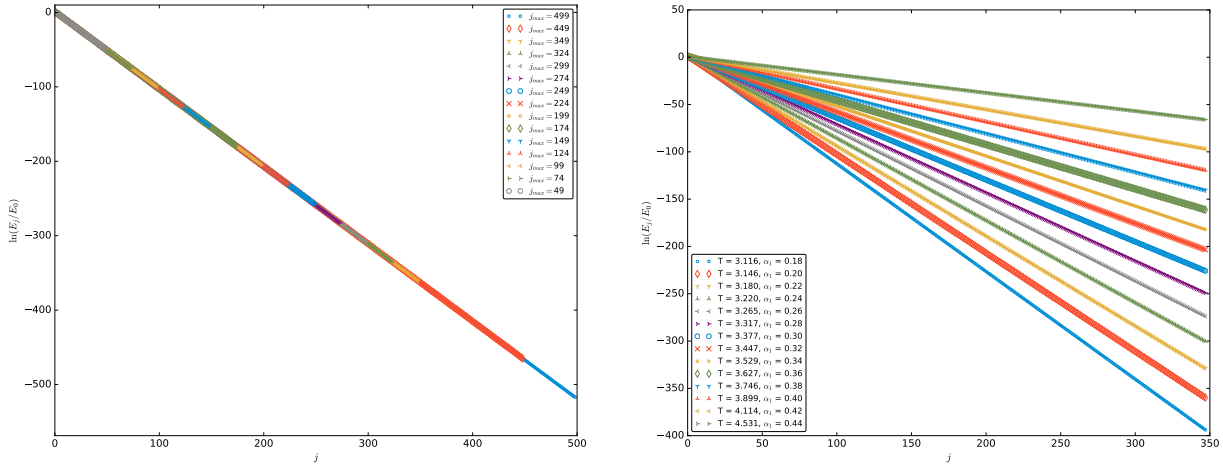

(a) *An overlay of QP solutions with* $\alpha_1 = 0.2$, *corresponding to* $T_0 \simeq 3.146$.

(b) *Families of QP solutions up to* $j_{max} = 350$.

Figure 1.1: *Energy spectra for various QP solutions.*

When examining the range of α_1 values that yield QP solutions, it was found that any small j_{max} QP solution could be extended to large j_{max} with proper seeding and sufficient computing power; that is, there seem to be no solutions that exist at low j_{max} that cease to exist at high j_{max}. However, a hard limit exists at the maximum α_1 value of $\alpha_1 = 0.442$, corresponding to a temperature of $T \simeq 4.643$. Above this limit, no QP solutions can be found even for j_{max} values as low as $j_{max} = 50$. Conversely, there is no lower limit to α_1 values; as $\alpha_1 \to 0$ with $\alpha_j > \alpha_{j+1}$, the TTF solution approaches the well-known single-mode solution.

1.5 High Temperature Perturbations

In [**?**], additional QP solutions were found by repeatedly perturbing away from existing solutions: the addition of some energy δE corresponds to the changes $\alpha_j \to \alpha_j + u_j$ and $\beta_j \to \beta_j + \theta_1 + \omega_j \theta_2$. The perturbed quantities are given by the system of linear equations

$$\delta E = 4 \sum_j \omega_j^2 \alpha_j u_j \tag{1.21}$$

$$\delta N = 4 \sum_j \omega_j \alpha_j u_j = 0 \tag{1.22}$$

$$\begin{aligned} 0 = {} & \omega_\ell \left(\alpha_\ell (\theta_1 + \omega_\ell \theta_2) + \beta_\ell u_\ell \right) + 6 T_\ell \alpha_\ell^2 u_\ell + 2 \sum_{i \neq \ell} R_{i\ell} (\alpha_i^2 u_\ell + 2 \alpha_i \alpha_\ell u_\ell) \\ & + 2 \sum_{i \neq \ell}^{\ell \leq i+j} \sum_{j \neq \ell} S_{ij(i+j-\ell)\ell} \left[u_i \alpha_j \alpha_{i+j-\ell} + u_j \alpha_i \alpha_{i+j-\ell} + \alpha_i \alpha_j u_{i+j-\ell} \right]. \end{aligned} \tag{1.23}$$

Therefore, by solving (1.21)-(1.23) for $\{u_j, \theta_1, \theta_2\}$, the existing QP solution can be updated and the process can be repeated.

For a standard QP solution with $\alpha_1 = 0.2$, the initial temperature is $T_0 = 3.146$. By applying the high temperature perturbation method described above, we are able to increase the temperature of the solution. However, this process must be examined with some scrutiny; applying repeated perturbations to a known solution does not guarantee the final result remains a valid solution. To investigate this further, we have implemented two high temperature solvers, both of which increment the energy of the system using (1.21)-(1.23) and are able to project back to the QP solution plane after a specified number of perturbations. However, the projection used by one solver takes an input α_1 value when solving the QP equation (1.19), while the other holds the temperature of the solution fixed during projection. To hold the temperature fixed, we use the definition of T and the freedom to rescale the α_j such that $\alpha_0 = 1$ to solve for α_1 via

$$\alpha_1^2 = \frac{1}{\omega_1 (T - \omega_1)} \left(\omega_0 (\omega_0 - T) + \sum_{j \geq 2} \omega_j (\omega_j - T) \alpha_j^2 \right) \tag{1.24}$$

It can easily be seen that α_1 will become singular when $T = \omega_1 = 5$ in AdS_4. Since we are inputting a value for the temperature T instead of a α_1, we are still solving a system of $j_{max} + 1$ equations for $j_{max} + 1$ unknowns.

1.5.1 Projections With α_1 as the Input

Let us first consider the results of the α_1 projection method, shown in figure 1.2. We have fixed the perturbation amount δE to 1% of the energy of the initial solution. Beginning with an $\alpha_1 = 0.44$ solution with low j_{max}, we apply repeated energy perturbations and project back to the QP solution plane with a frequency of once per 5 temperature iterations (see appendix 1.C for further discussion on projection frequency and energy perturbation value). Figure 1.2a shows the resulting values of α_1 and T during these perturbations. We see that α_1 approaches an attractor solution of $\alpha_1 \simeq 0.43$ with $T \simeq 4.3$. The energy perturbations between the projections are insufficient to escape this local minimum so that repeated projections return the same solution. However, when the projection frequency is decreased to once every 20 iterations, the attractor solution is able to be bypassed (variations of the projection frequency and energy perturbations are discussed in appendix 1.C). Note that as the iteration number increases, we actually see a *decrease* in α_1 value while the temperature continues to increase. At iteration 150 in figure 1.2b, there is a cusp in α_1 and a discontinuity in the temperature. After several hundred iterations, α_1 becomes negative.

Let us examine the energy spectra these solutions. In figure 1.3a we see that when we choose a high projection frequency, the resulting energy spectra do not deviate far from the initial solution (using the α_1 projection method) in either shape or temperature. We denote solutions found by this method as "threshold temperature" solutions. The values of the threshold temperature T_{th} is robust against increases in j_{max} and is independent of the starting value of α_1, as shown in table 1.1.

When the projection frequency is decreased, the temperature is able to exceed T_{th}. However, as seen in figure 1.3b, projections back to the QP plane give $\alpha_1 < 0$ and an energy spectrum that is no longer C^1 differentiable (*c.f.* spectra of iterations 120 and 180). This in itself is not necessarily

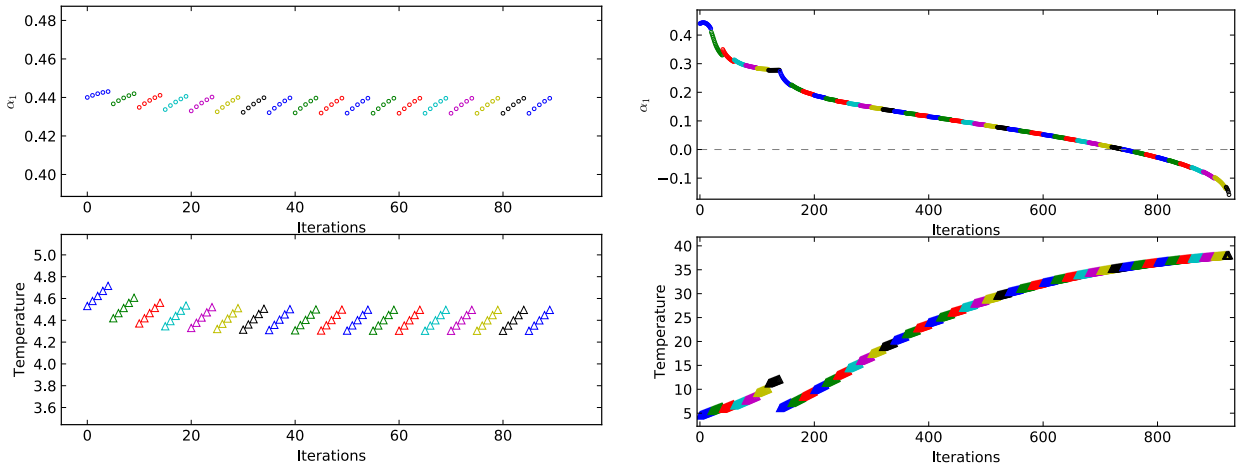

(a) *Applying repeated energy perturbations to the initial solution with* $\alpha_1 = 0.44$*, projecting back to the QP plane every five iterations.*

(b) *The same QP solution, but projecting back to the QP plane every 20 iterations.*

Figure 1.2: *The results of projecting a* $j_{max} = 50$*,* $\alpha_1 = 0.44$ *solution back to the QP plane at various frequencies during high temperature perturbations. Colour changes indicate that the solution has been projected back to the QP plane.*

a breakdown of the quasi-periodic nature of the solution, as $\alpha_j < 0$ if $\beta_j \tau = (2n+1)\pi$ for $n \in \mathbb{N}^0$. However, upon examining the condition number of the matrix formed by (1.21)-(1.23), we find that in fact the problem becomes ill-conditioned. This results in a absolute value of u_i that is greater than α_i; that is, the perturbative condition required to derive the system of linear equations (1.21)-(1.23) breaks down. For many prospective high-temperature solutions, this break-down of the perturbative condition is signalled by the loss of C^1 differentiability in the energy spectrum due to the values of α_j becoming negative.

1.5.2 Projections at Constant Temperature

We again use a series of small energy perturbations to seek high-temperature QP solutions, this time using a constant-temperature projection method at regular intervals. Starting from a standard

j_{max}	T_{th}	Iterations
50	4.30344575697724e+00	350
75	4.30344544264076e+00	210
100	4.30344544023857e+00	540
150	4.30344544024198e+00	280
200	4.30344544023915e+00	300

Table 1.1: *Values of the threshold temperature T_{th} for QP solutions with given j_{max}. Also included is the number of iterations applied (projecting back to the solution plane after every five iterations).*

$\alpha_1 = 0.44$ QP solution, perturbations are applied to increase the temperature. After five increments, the temperature is calculated and used as the input to the second nonlinear solver. This ensures that the temperature is not changed when projecting back to the solution plane. Goal temperatures of $T = 5.5$, 6.0, and 7.0 were chosen – when the solution reached or exceeded this temperature, it would be projected back to the QP plane and the perturbations would cease. The resulting spectra for each temperature goal over several choices of j_{max} are shown in figure **??**. It is worth noting that $j_{max} = 250$ spectra are not included for temperature goals of $T = 6.0$ and 7.0 because the constant-temperature projection failed to find a solution.

Recall that solutions must be robust in the limit of $j_{max} \to \infty$ in order to be considered solutions to the full TTF theory. While the upper panel of figure **??** suggests that solutions with temperatures at or near $T = 5.5$ can be constructed in the large-j_{max} limit, it is clear that goal temperatures of $T = 6.0, 7.0$ do not support solutions to the full TTF theory. In fact, when solutions were not projected back to the QP plane at regular intervals during the energy perturbations, no solutions at all could be found when the temperature was held fixed. It would seem that the domain of high temperature QP solutions is restricted to a narrow region near the QP plane defined by (1.19).

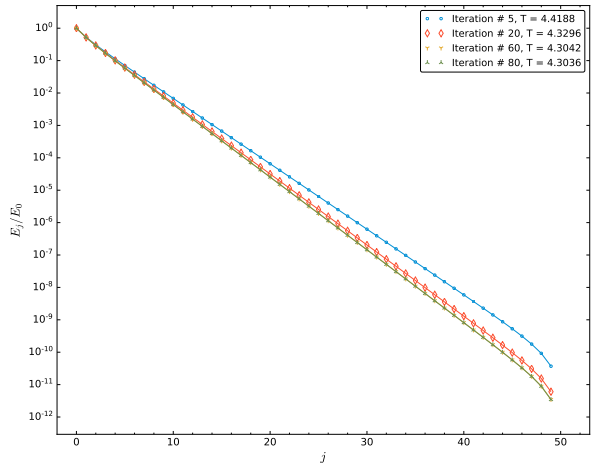

(a) *Energy spectra when projecting back to the QP solution plane every 5 iterations for an initial* $\alpha_1 = 0.44$*, QP solution (see figure 1.2a for temperature and* α_1 *as a function of iteration).*

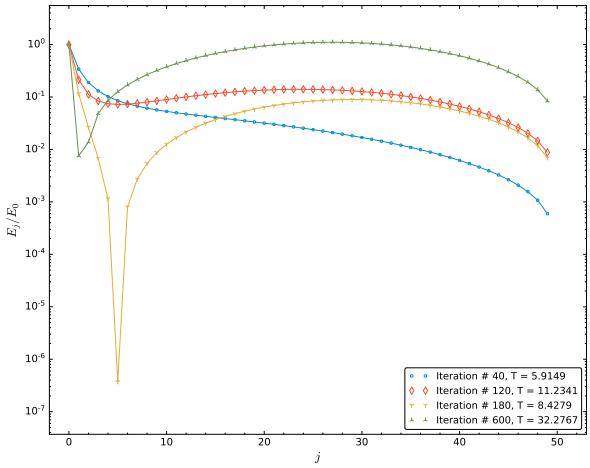

(b) *The same initial QP solution as figure 1.3a is used, but is projected back to the QP plane every 20 iterations.*

Figure 1.3: *Comparing energy spectra of high-temperature perturbations of an* $\alpha_1 = 0.44$ *QP solution that have been projected back to the QP plane at different frequencies.*

1.5.3 Building High-Temperature Solutions

In figure **??** we see that continuous spectra exist for goal temperatures of $T = 6.0$ and 7.0 when $j_{max} = 50$. It is therefore reasonable to consider whether a high temperature, low j_{max} solution could be extended to a high temperature, high j_{max} solution using a fitting procedure similar to that used in § 1.4.1 to find quasi-periodic solutions. Instead of fitting α_j values away from the highest modes, we instead apply the tail fitting the final 5 modes and use the fit to generate seed values for a $j_{max} + 5$ solution. We see in figure 1.4b that this method results in spectra where energy becomes increasingly concentrated in high-j modes. In fact, for solutions with $j_{max} \geq 90$, and equal or greater amount of energy resides in the high-j modes than in the zero-mode. These solutions are not robust as $j_{max} \to \infty$ and therefore are not solutions to the TTF equations.

1.5.4 Stability of QP Solutions

Having identified QP solutions that are robust in the limit of $j_{max} \to \infty$, as well as a class of higher temperature solutions found from incremental perturbations about QP solutions, we can now ask how these solutions would evolve within the perturbative description. In particular, we wish to examine possible direct and inverse energy cascades in these quasi-periodic solutions, and determine if they continue to represent stable data. The cascades of energy between length scales will be evident in the spectra. Indirect observations of stability can be made through the value of the Ricci scalar at the origin, since large absolute values and/or rapid increases in scalar curvature often indicate instability in numerical simulations [**?**].

Another indicator of possible collapse and/or violation of the perturbative approximation is the growth of residuals when the TTF solutions are substituted into the Einstein equations. The residuals are calculated by reconstructing the time dependence of the scalar field and its derivatives using the amplitude-phase variables, and comparing the $\mathcal{O}(\epsilon^2)$ values of the derivatives of the metric functions in (1.5)-(1.6). In particular, using the numerical values of the amplitude-phase variables A_j and B_j, (1.11) gives the value of the leading-order scalar field contribution, $\phi_1(t,x)$. The $\mathcal{O}(\epsilon^2)$ contribution to the derivatives of metric functions come from

$$\partial_x \delta_2(t,x) = -\sin(x)\cos(x)\left((\partial_x\phi_1)^2 + (\partial_t\phi_1)^2\right) , \tag{1.25}$$

$$\partial_x A_2(t,x) = -\frac{1-d+\cos(2x)}{\sin(x)\cos(x)}(A_2 - 1) - \sin(x)\cos(x)\left((\partial_x\phi_1)^2 + (\partial_t\phi_1)^2\right) , \tag{1.26}$$

$$\text{with } A_2(t,x) = -\frac{\cos^d(x)}{\sin^{d-1}(x)}\int_0^x \tan^{d-1}(y)\left((\partial_t\phi_1)^2 + (\partial_x\phi_1)^2\right) dy\,. \tag{1.27}$$

The L^2-norm of the differences between (1.24)-(1.25) and (1.5)-(1.6) would constitute the residuals of the Einstein equations. However, while the leading-order contribution to the residuals is $\mathcal{O}(\epsilon^4)$, there are in fact higher order terms that enter into the calculation of $\partial_t\phi$. A careful evaluation of the constraints would therefore include calculating the $\mathcal{O}(\epsilon^4)$ term in the metric function $A(t,x)$ so that the product $A(\Phi^2+\Pi^2)$ would include terms $\mathcal{O}(\epsilon^6)$. Instead, we limit our focus to examining only

the difference between (1.5) and (1.24), which does not suffer from higher-order contributions. The examination of residuals is taken as a suggestion of how well a TTF solution continues to satisfy the Einstein equations throughout its evolution, with the understanding that growing residuals would indicate that higher order terms in the perturbative expansion are becoming relevant. See figure **??** for an example.

1.6 Time Evolution of Quasi-Periodic Solutions

The weakly turbulent behaviour of the scalar field in the TTF is captured by the $\mathcal{O}(\epsilon^2)$ renormalization group flow equations (1.15)-(1.16). Having identified different families of quasi-periodic solutions, we wish to evolve these solutions and examine the direct and inverse cascades responsible for balancing the flow of energy between long and short length scales. Furthermore, we may also be able to identify inaccessible solutions by orbiting around a time-independent solution and attempting to project back to the QP plane. To achieve these aims, we use numerical methods first described by [**?**] and take solutions discussed in § 1.4 as initial data.

1.6.1 Low-temperature QP data

Let us consider the evolution of a "typical" QP solution: a solution to (1.19) with $\alpha_1 = 0.2$ and $j_{max} = 100$, corresponding to a temperature of $T = 3.146$. Choosing an amplitude of $\epsilon = 0.01$ (note that the TTF equations are invariant under $\mathcal{A}(\tau) \to \epsilon\, \mathcal{A}(\tau/\epsilon^2)$ and so the value of ϵ does not change the physics), figure 1.7 shows the evolution of the fraction of the total energy per mode. We see that energy in the lowest-j modes remains constant over the duration of the evolution, while the fraction in the highest-j modes increases after $\tau \simeq 0.3$. Similar behaviour is observed for higher j_{max} solutions and over values of $0.2 \leq \alpha_1 \leq 0.44$. Given the scale of the energy in the modes $j \geq 96$, the growing energy fractions in these modes can mainly be attributed to numerical errors rather than direct energy cascades.

We may also ask: does a given quasi-periodic solution remain unique under evolution? That is, will the solution project back to itself during its evolution? To answer this, we evolve the same low-temperature, QP solution and take the spectra at different times as seed values for projecting back to the QP plane. We observe that these solutions continue to be projected back to themselves at all times during the evolution, and that the resulting solutions solve the QP equation (1.19) to a high degree of accuracy (see figure 1.9a).

In an effort to extend the space of QP solutions, another method can be used to find solutions that exist nearby known QP solutions – but are not accessible through perturbative or conventional seeding methods: padding a given quasi-periodic solution with extra modes that are initially set to zero. Upon amplitude-phase evolution via (1.15)-(1.16), the energy in the lower-j modes will flow into the higher-j modes and a new quasi-periodic solution may be found, albeit with the same temperature. In figure 1.10, we construct initial data out of a known $j_{max} = 100$, $T \simeq 3.14$ solution by padding the data with zeros up to $j_{max} = 200$. As in the case of unpadded QP solution, the fraction of the total energy in the first four modes does not vary significantly during the evolution and the highest modes accumulate some numerical error before levelling off. Despite the somewhat normal profile of the spectra of padded QP solution (shown in figure 1.10d) and the relatively low value of the Ricci scalar (see figure **??**) – we find that intermediate solutions during the evolution in fact *do not* project back to the QP plane after roughly halfway through the evolution. Evaluating the residuals of the Einstein equations, we find relative residuals on the order $\sim 5 \times 10^{-1}$, indicating a drift away from the quasi-periodic initial data (*c.f.* figure **??**). It remains to be seen whether such profiles would be stable in the fully nonlinear system. Finally, we may ask how far away from the solution plane we can move by padding a known QP solution with an incremental number of zeros. Beginning with the same $j_{max} = 100$ QP solution, we pad with only five modes this time. Despite a QP solution with $j_{max} = 105$ already being known, the evolution did not result in the padded solution approaching the known solution. Furthermore, using intermediate spectra of the padded solution as seed values for projecting back to the QP plane did not result in new QP solutions at any point during the evolution.

1.6.2 High-Temperature QP Data

We now apply the same amplitude-phase evolution procedure to threshold and possible high-temperature QP data. First, consider a threshold temperature solution with $j_{max} = 100$ and $T \sim 5.4$. Such a solution was demonstrated in figure **??** to be within the regime of solutions accessible through repeated energy perturbations that persisted as $j_{max} \to \infty$. In figure 1.12 we show the energy spectrum at various times during the evolution, as well as the fractional energy per mode. Because of the initial profile of solutions with these temperatures, there is a much higher fraction of the total energy in the higher modes; therefore, the accumulation of numerical errors that were present in low-temperature solutions are not seen here. Close inspection of figure 1.12b, which shows the fractional energy in the high frequency components of the scalar field, reveals small oscillations in E_j/E_{tot} as energy undergoes direct and inverse cascades between high and low frequency components. However, these oscillations are not sufficient to produce a qualitative change in the full energy spectrum, as shown in figure **??**. Finally, examination of the absolute value of the scalar curvature at the origin in figure **??** shows that the large initial value of $|\mathcal{R}|$ oscillates rapidly during evolution. Since the TTF description is inherently stable, the curvature will never become infinite; however, large values of curvature with rapid oscillations are good indicators of instability. It would be interesting to use such a solution as initial data for evolution in the fully nonlinear system to see if stability is maintained over the perturbative timescale.

As in the case of low-temperature QP solutions, we wish to expand the space of possible solutions by padding threshold data with extra modes initially set to zero. Consider padding the threshold temperature solution of $T \sim 5.4$ from $j_{max} = 100$ to $j_{max} = 200$ with $\alpha_j = 0$ for $j > 99$. Figure **??** demonstrates that after evolving in time there are indications of large scale energy transfer amongst modes with higher frequencies. Interestingly, the magnitude and oscillation frequency of the Ricci scalar at the origin is significantly decreased compared to the $j_{max} = 100$ threshold solution. When compared against the known solution of the same temperature when $j_{max} = 200$, figure 1.20 indicates that the padded solution may not approach the known threshold solution and instead may have

produced a distinct, but equal temperature, solution.

It has been suggested that high-temperature QP solutions should exist in a continuous region of temperature space $T \in [T_{min}, T_{max}] = [d, 2j_{max} + d]$ and that perturbing a low-temperature QP solution to a temperature above T_{th} before implementing perturbative increases in energy followed by regular projections allows for all such solutions to be found. However, we have found that high temperature solutions produced using regular projections back to the solution plane are not robust as $j_{max} \to \infty$ and therefore do no constitute physical solutions. The question of whether new families of solutions can be accessed by alternative methods bears consideration.

First, we consider applying a similar fitting technique to threshold temperature data as was used to extend low-temperature QP solutions. In this case, values were taken from the middle of high temperature solutions with $j_{max} = 50$ and fit with an exponential function (see figure 1.A.1 for a similar procedure with tail values) over 10 modes. The new values α_{fit} were then combined with the existing values so that $\alpha_j = \langle \alpha_{j<j_{mid}}, \alpha_{fit}, \alpha_{j>j_{mid}} \rangle$. This would extend the high temperature solution by 10 modes and would slightly increase the temperature, hopefully providing a good seed for the constant-temperature nonlinear solver. However, no solutions were found using this method, starting either with $j_{max} = 50$, $T > 5.5$ data, or $j_{max} = 200$, $T = 5.5$ data.

Next, we consider perturbing up to an intermediate temperature $T_{th} \ll T_{int} < T_{max}$ before attempting to project back to the QP plane using the T_{int} data as seed values. In particular, we repeatedly perturb a $T \sim 4.5$ solution using the method described in § 1.4.2 to a temperature of $T_{int} = 20$ without projecting back to the QP plane *at any point*. For $j_{max} \lesssim 100$, projection back to the solution plane finds a new solution with $T < T_{int}$ that – much like the spectra shown in figure 1.3b – loses C^1 differentiability. Furthermore, the fractional energy in the low-frequency modes oscillates rapidly over several orders of magnitude during the evolution, and the Ricci scalar reaches values $\mathcal{O}(10^6)$; these solutions are almost certainly not quasi-periodic. The same result is found for high temperature solutions created by fitting tail data (see figure 1.4b for example spectra). Finally, for $j_{max} \geq 100$, projection back to the QP solution plane once $T = T_{int}$ fails entirely. Thus, the space of QP solutions is greatly diminished with $T_{max} \ll 2j_{max} + d$.

1.7 Discussion

We have explored the space of quasi-periodic solutions within the weakly turbulent description of a massless scalar field in AdS_4. Using the conserved quantities E and N, we constructed families of quasi-periodic solutions that were distinguished by the temperature $T = E/N$ for different choices of the truncation value j_{max}. We have demonstrated that low temperature QP solutions, i.e. those that are immediately accessible by solving (1.17) for a given α_1 such that $\alpha_1 < \alpha_0 = 1$, can be extended to arbitrarily large j_{max} values, and therefore constitute solutions to the TTF theory. We have also examined high temperature QP solutions, which are found by perturbing low temperature solutions by δE while keeping N fixed. We found that a high temperature solutions were robust in the limit of large j_{max} only for temperatures close to the solution plane; solutions with even $3T_0/2$, where T_0 is the highest temperature achievable without applying the perturbative method, did not persist as j_{max} was increased. Several alternative methods for generating QP solutions up to $T_{max} = 2j_{max} + d$ were explored, none of which yielded solutions to the untruncated TTF system.

By construction, TTF solutions are stable against gravitational collapse and therefore evolution within the TTF description will not produce a singularity. However, there are several indicators for instability in the fully nonlinear theory: the value of the Ricci scalar at the origin, the growth higher-order contributions to the lapse function δ, and rapid growth/oscillations in the energy of high frequency modes. Using these measures, we have seen that low-temperature QP solutions continue to solve the TTF system despite the accumulation of numerical errors. At late times in their evolution, these solutions can be projected back to the QP solution plane without altering their energy spectra. Beginning with a low-temperature QP solution of j_{max} initial modes, we padded the solution to $2j_{max}$ with zero-energy modes and observed its evolution. The inclusion of extra modes caused an isothermal drift away from the known $2j_{max}$ QP solution, and resulted in values that could not be projected back to the QP plane. In such cases, the scalar curvature became oscillatory with values ranging up to 20 times the initial curvature.

High temperature solutions of several varieties were evolved within the TTF theory. When solu-

tions with temperatures at or near the threshold temperature were examined, the fractional energy distribution remained roughly constant with some evidence of direct and inverse energy cascades at high mode numbers. Despite relatively large values of the Ricci scalar, the ultimate stability or instability of such solutions over timescales of $t \sim \epsilon^{-2}$ in the fully nonlinear theory remains unclear. Padding threshold solutions with zero-energy modes once again produced isothermal drift during evolution and did not converge to the known QP solution for that temperature and number of modes. These solutions, however, exhibit slow oscillations of scalar curvature over a narrow range of values, hinting that stability over perturbative timescales in the nonlinear theory. Finally, we did not find any evidence for families of QP solutions in a continuous region of temperature space up to $T_{max} = 2j_{max} + d$. We demonstrated that low-j_{max} solutions with $T \gg T_{th}$ could be constructed, but were not robust as $j_{max} \to \infty$ and therefore were not true solutions to the TTF description. Rather, only solutions with temperatures $T \gtrsim T_{th}$ could be extended to large j_{max} values. The nature of the threshold temperature T_{th} is not totally understood; we conjecture that the singular nature of $\alpha_1(T)$ in (**??**) when $T = \omega_1 = d + 2$ produces a local maximum in the Hamiltonian and that the nearest minimum corresponds to solutions with $T = T_{th}$. By perturbing sufficiently far from the QP plane, one is able to overcome this maximum and will project to the next set of QP solutions whose temperature can be as high as $T = 5.5$, as shown in figure **??**. Above this temperature, the Hamiltonian has no stable minima and therefore QP solutions do not exist. A more complete analysis of the Hamiltonian as a function of temperature will be required for this interpretation to be confirmed.

With respect to the overall stability of AdS_4, as well as the interpretation of stable data in the bulk as non-thermalizing states in the boundary theory, we have found that the space of stable initial data most likely does not include families of quasi-periodic solutions with high temperatures. This means that quasi-periodic initial data must be closer to single-mode and nearly single-mode data to remain stable over perturbative timescales than previously thought; that is, data with high fractional energies in high mode numbers is not able to resist collapse as effectively, even through the balancing of energy cascades. We have focused entirely on solutions where the dominant energy

contribution is in the $j = 0$ mode – these solutions would generally offer the greatest range of stable initial data. However, other configurations are possible where the dominant energy contribution is in the j_r mode, with $r \neq 0$. As shown in [**?**], as r increases, the range of quasi-periodic data decreases. In such cases, we expect even greater restrictions on the range of temperatures that characterize QP solutions of the full Two-Time Formalism.

Acknowledgments The work of ND is supported in part by a Natural Sciences and Engineering Research Council of Canada PGS-D grant to ND, NSF Grant PHY-1606654 at Cornell University, and by a grant from the Sherman Fairchild Foundation. The work of BC and AF is supported by the Natural Sciences and Engineering Research Council of Canada Discovery Grant program. This research was enabled in part by support provided by WestGrid (www.westgrid.ca) and Compute Canada Calcul Canada (www.computecanada.ca).

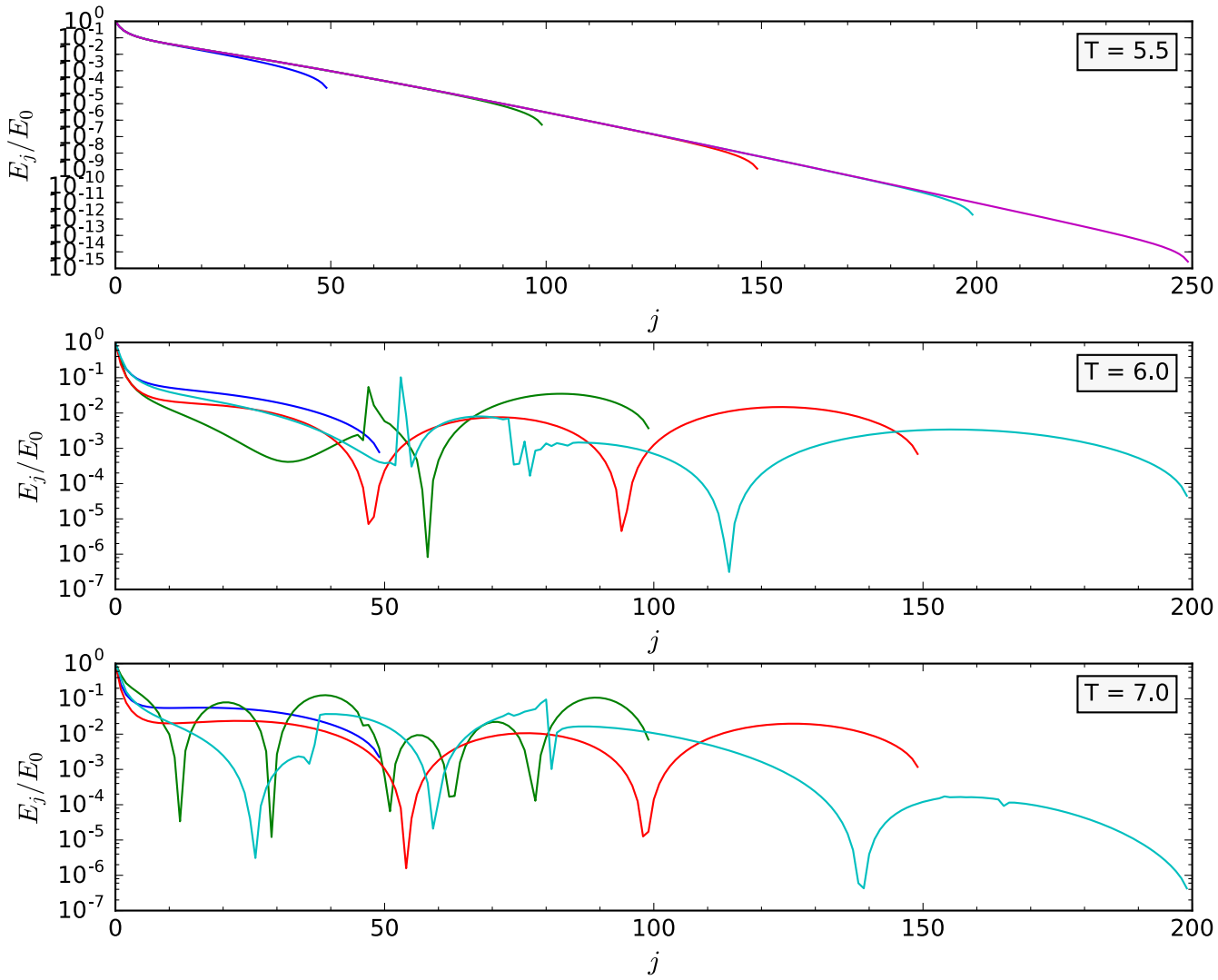

Figure 1.4: *Finding high temperature QP solutions using repeated perturbations with regular projections back to the QP plane.*

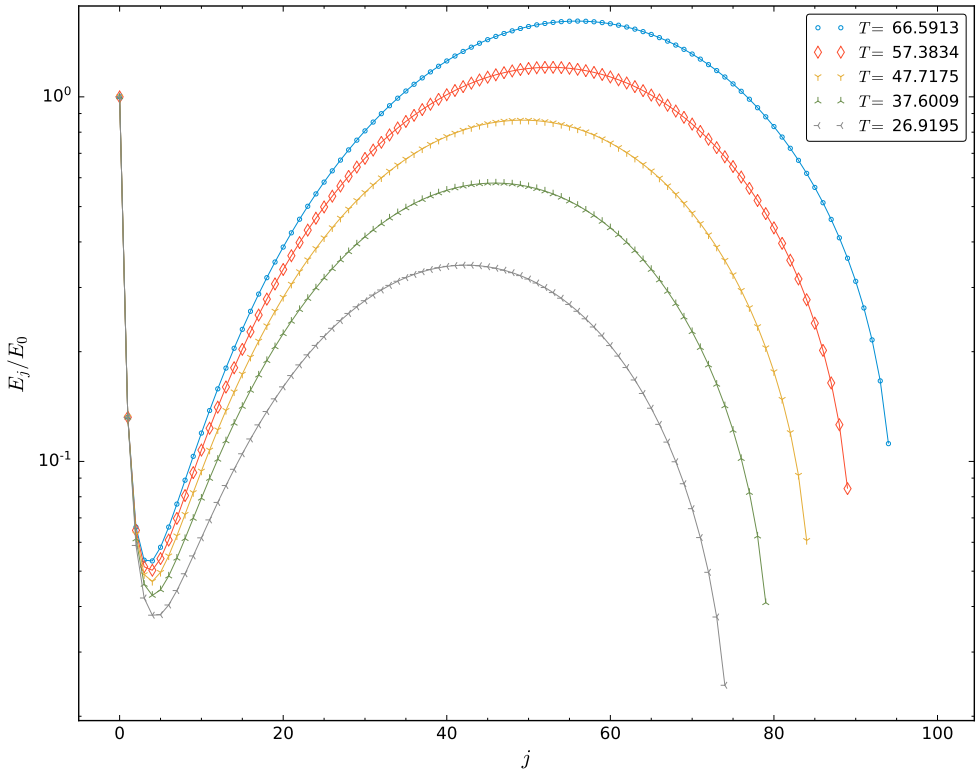

Figure 1.5: *Extending a high temperature, low j_{max} solution to higher temperatures by fitting the final 5 modes and generating seed values.*

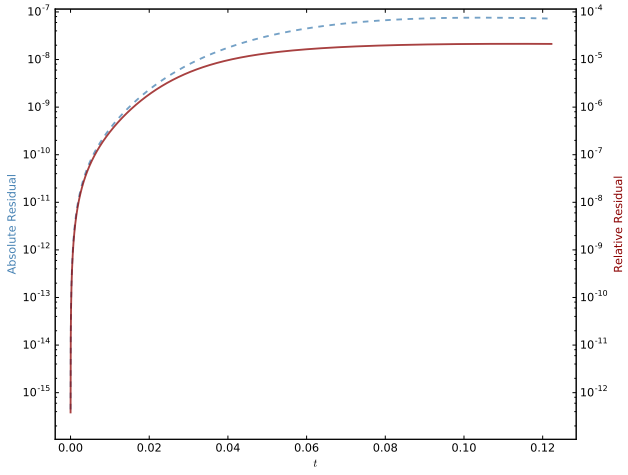

Figure 1.6: *Absolute and relative residuals of the Einstein equations during evolution of a low-temperature, $j_{max} = 100$ QP solution with $\epsilon = 0.001$.*

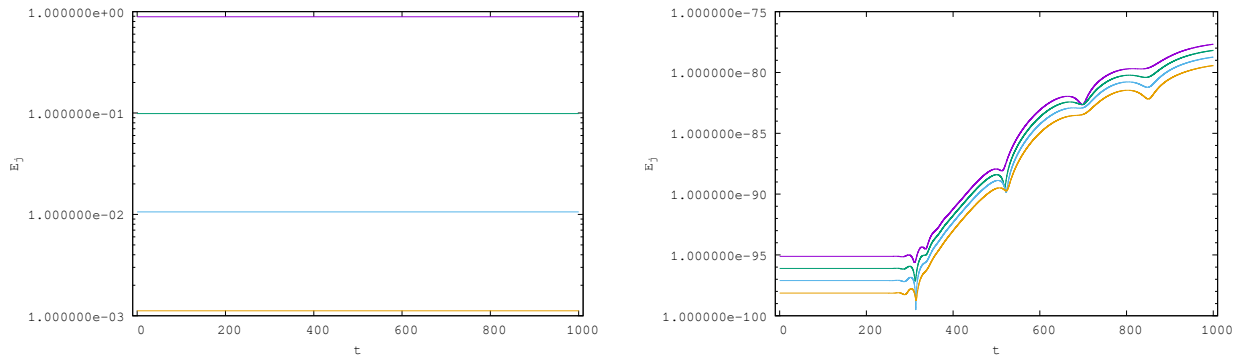

(a) *From top to bottom:* $j = 0, 1, 2, 3$ *(purple, green, blue, orange).*

(b) *From top to bottom:* $j = 96, 97, 98, 99$ *(purple, green, blue, orange).*

Figure 1.7: *Fraction of the total energy in each mode during evolution of an* $\alpha_1 = 0.2$*,* $j_{max} = 100$*, QP solution with* $\epsilon = 0.01$*.*

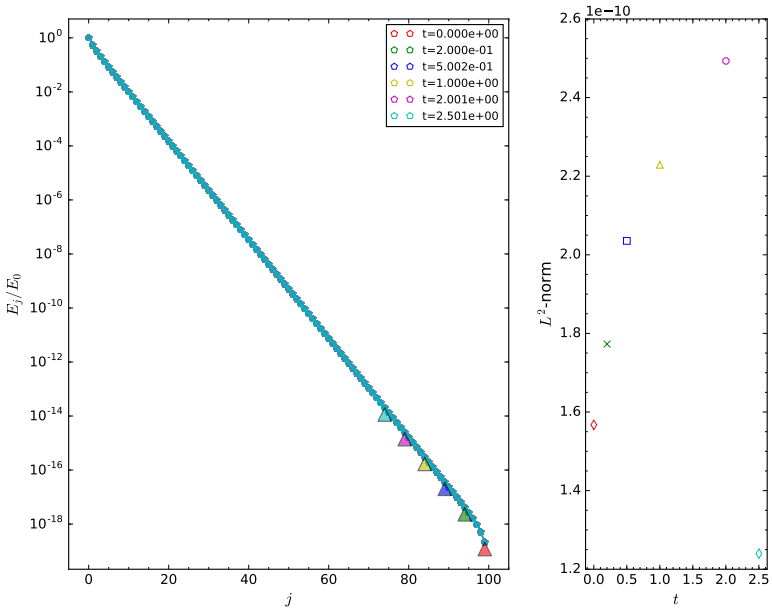

Figure 1.8: *Left: Projecting a low-temperature solution back to the QP plane during its evolution. Arrows are oriented from amplitude/phase seed values (circles) to QP plane projections (pentagons). Right: the* L^2*-norms of the projected solutions at* $t \simeq 0.0, 0.2, 0.5, 1.0, 2.0, 2.5$ *(red diamond, green cross, blue square, yellow triangle, magenta circle, blue diamond).*

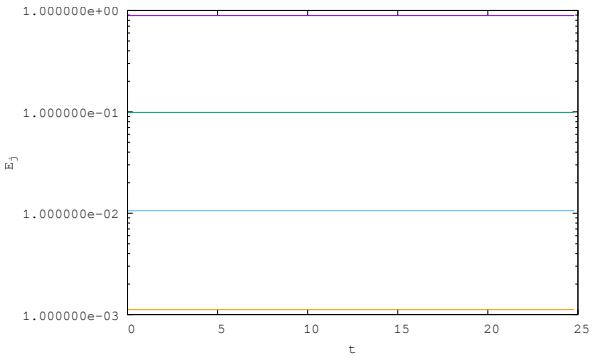

(a) *The evolution of the first four modes of the padded QP solution:* $j = 0, 1, 2, 3$ *(purple, green, blue, orange).*

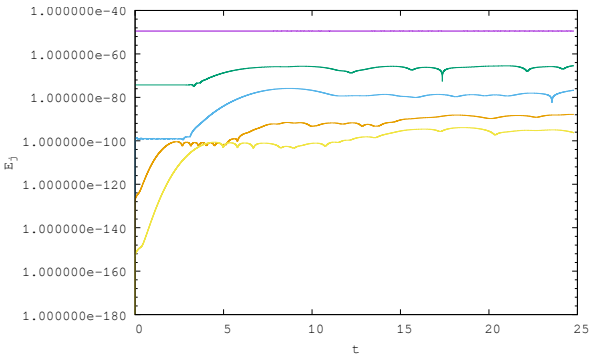

(b) *Comparing the evolution of a selection of modes:* $j = 50, 75, 100, 125, 150$ *(purple, green, blue, orange, yellow).*

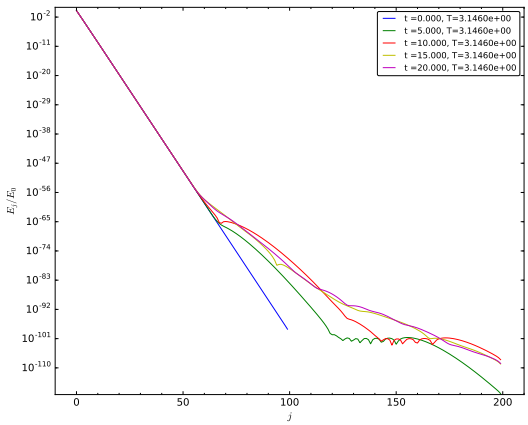

(c) *The total spectrum of the padded QP solution as a function of time.*

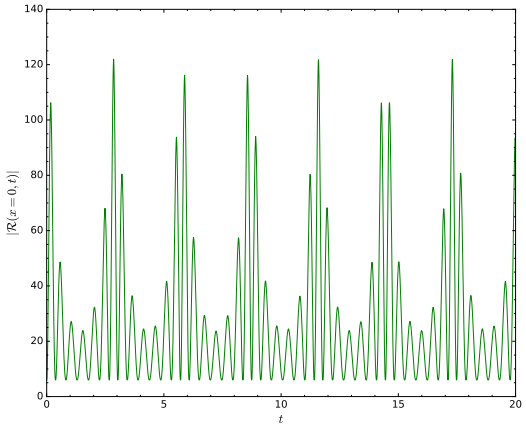

(d) *The Ricci scalar at the origin as a function of time.*

Figure 1.9: *The evolution of the padded QP solution for* $\alpha_1 = 0.2$ *and* $j_{max} = 200$*, with amplitude* $\epsilon = 0.27$*.*

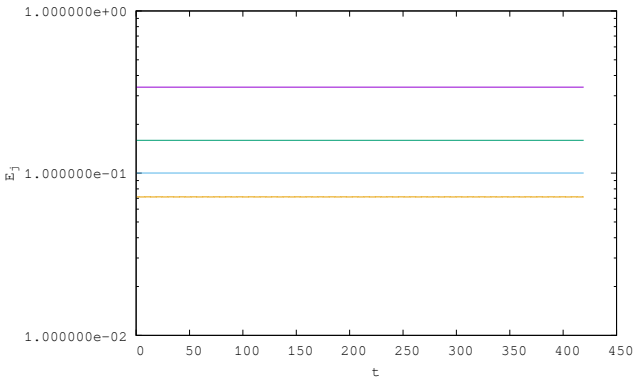

(a) $j = 0, 1, 2, 3$ *(purple, green, blue, orange).*

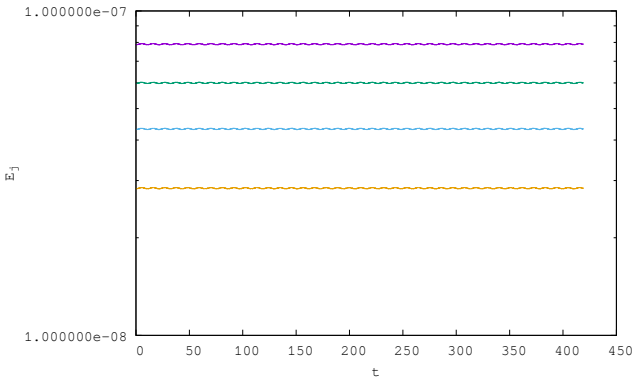

(b) $j = 96, 97, 98, 99$ *(purple, green, blue, orange).*

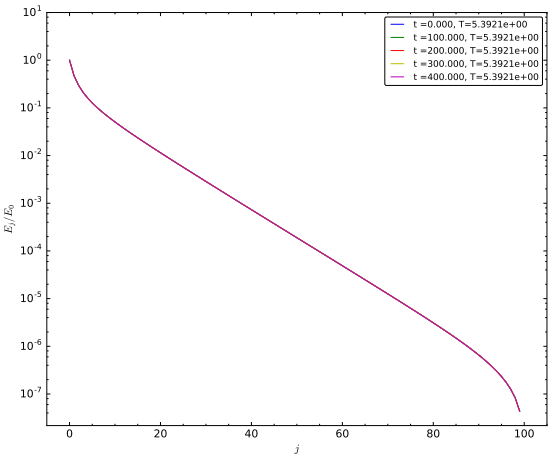

(c) *The energy spectrum during evolution.*

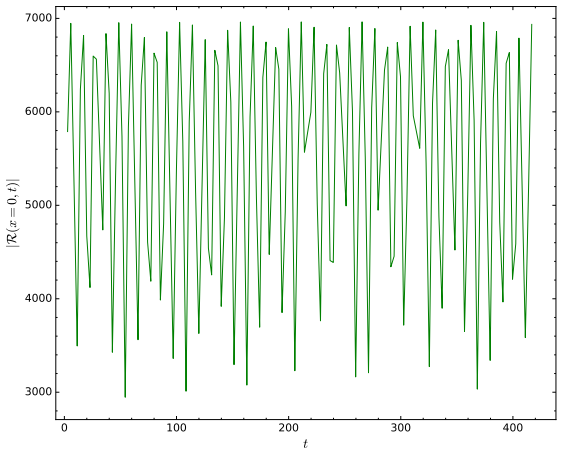

(d) *The upper envelope of the scalar curvature.*

Figure 1.10: *The evolution of a threshold temperature solution with* $T \sim 5.4$ *with* $\epsilon = 0.1$ *over* $\tau \in [0, 4.25]$.

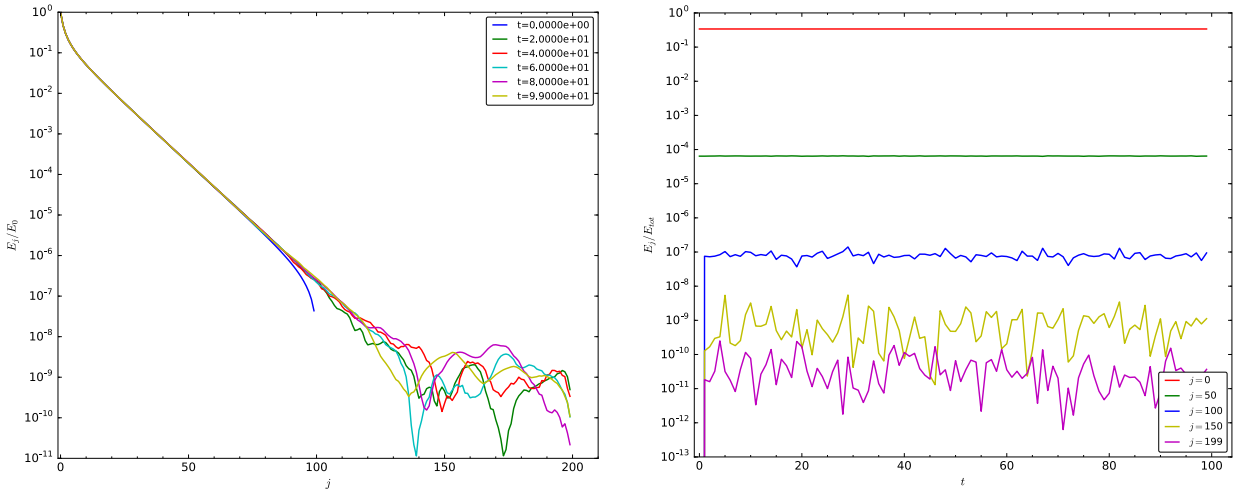

Figure 1.11: *The threshold temperature solution shown in figure 1.12 is padded with 100 extra modes and evolved with* $\epsilon = 0.1$.

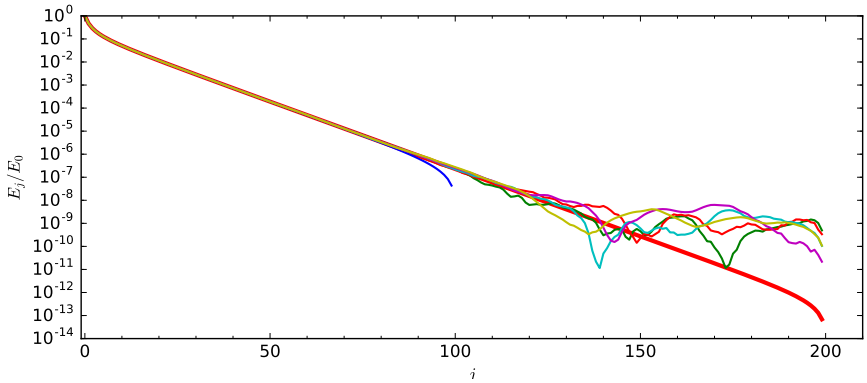

Figure 1.12: *Overlay of the known threshold temperature solution for* $j_{max} = 200$ *(thick red line) with the spectra in figure* **??**.

Appendix

1.A Seeding Methods For Non-Linear Solvers

While it was originally proposed by [**?**] that the appropriate seed value for nonlinear solvers be given by the exponential relation ($j > 1$)

$$\alpha_j \sim \frac{3e^{-\mu j}}{2j+3} \tag{1.28}$$

in AdS_4, where $\mu = \ln(3/5\alpha_1)$, as j_{max} increased, the seed values diverged significantly from the true solutions (see figure 1.A.1 for a comparison between known QP solutions and the seeds generated by (1.27)). Although this profile was sufficient for low j_{max} solutions, above $j_{max} \gtrsim 150$, (1.27) no longer provided an adequate starting guess. To overcome this problem, exponential fitting was applied to the tail values of a known QP solution with lower j_{max}. Using this exponential fit, the data was extrapolated to a higher j_{max}.

Care was taken to avoid edge effects due to truncation when choosing the points that constituted the tail of the data. To illustrate the variance of the solution with truncation, we examine a fixed α_j value over a variety of j_{max}, starting with $\alpha_j = \alpha_{j_{max}}$. In table 1.A.1 we see that the value of α_{50} for QP solutions with $\alpha_1 = 0.2$ becomes impervious to truncation effects once $j_{max} > 55$.

To err on the side of caution, the modes $[j_{max} - 30,\ j_{max} - 10]$ were used from each QP solution to provide more accurate seed values for $j_{max} + 25$ solutions. See figure 1.A.2a for a comparison of seed values generated by tail fitting to actual QP solutions. The solutions found using this method

j_{max}	α_{50}
50	1.74597252e-26
51	1.82668391e-26
52	1.83346256e-26
53	1.83408260e-26
54	1.83414138e-26
55	1.83414706e-26
60	1.83414768e-26
65	1.83414768e-26
70	1.83414768e-26
75	1.83414768e-26

Table 1.A.1: *α_{50} values for various j_{max} QP solutions.*

of seeding versus those found from the seeding given in (1.27) had relative differences on the order of 10^{-14} (see figure 1.A.2b).

1.B Auxiliary Integrals For Calculating the T, R, S Coefficients

The auxiliary coefficients X, Y, W, W^*, A, and V allow the symmetries of the T, R and S coefficients to be more easily recognized and therefore reduce the number of total calculations involved in determining (1.34) - (1.36). These auxiliary coefficients are written simply in terms of the eigenfunctions

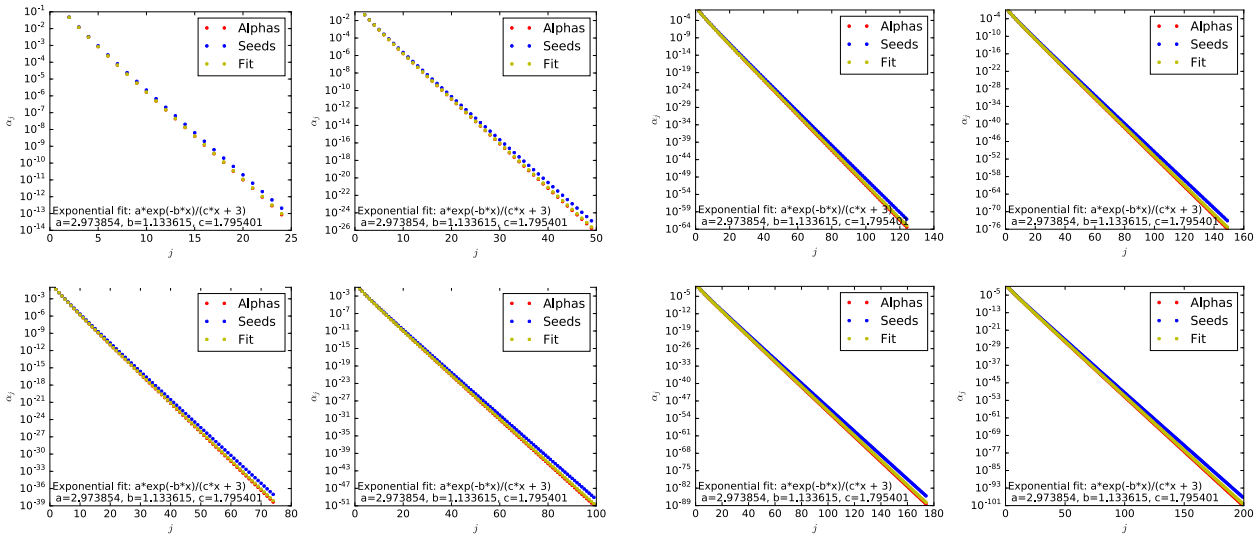

(a) $\alpha_1 = 0.2$ *QP solutions for* $j_{max} \in [25, 100]$. **(b)** $\alpha_1 = 0.2$ *QP solutions for* $j_{max} \in [140, 200]$.

Figure 1.A.1: *A comparison of seeds predicted by* (1.27) *to known QP solution. Also included for comparison are the results of fitting the QP solutions to a generic exponential fit.*

in (1.9) and their derivatives. Explicitly, they are

$$X_{ijk\ell} = \int_0^{\pi/2} dx\, e_i'(x) e_j(x) e_k(x) e_\ell(x) \sin(x) \cos(x) \left(\tan(x)\right)^{d-1} \tag{1.29}$$

$$Y_{ijk\ell} = \int_0^{\pi/2} dx\, e_i'(x) e_j(x) e_k'(x) e_\ell'(x) \sin(x) \cos(x) \left(\tan(x)\right)^{d-1} \tag{1.30}$$

$$W_{ijk\ell} = \int_0^{\pi/2} dx\, e_i(x) e_j(x) \sin(x) \cos(x) \int_0^x dy\, e_k(y) e_\ell(y) \left(\tan(y)\right)^{d-1} \tag{1.31}$$

$$W^*_{ijk\ell} = \int_0^{\pi/2} dx\, e_i'(x) e_j'(x) \sin(x) \cos(x) \int_0^x dy\, e_k(y) e_\ell(y) \left(\tan(y)\right)^{d-1} \tag{1.32}$$

$$A_{ij} = \int_0^{\pi/2} dx\, e_i'(x) e_j'(x) \sin(x) \cos(x) \tag{1.33}$$

$$V_{ij} = \int_0^{\pi/2} dx\, e_i(x) e_j(x) \sin(x) \cos(x)\,. \tag{1.34}$$

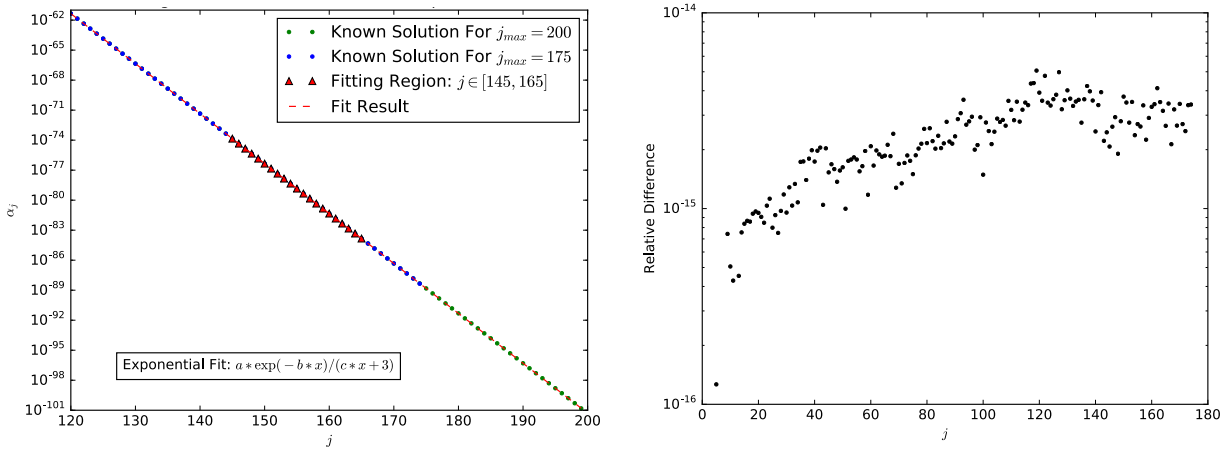

(a) *Fitting the tail of the $j_{max} = 175$ spectrum to construct a seed for $j_{max} = 200$ at fixed $\alpha_1 = 0.2$. Also included is actual QP spectrum for $j_{max} = 200$.*

(b) *Relative difference between $\alpha_1 = 0.2$ QP solutions found using tail-fitting and those from the exponential profile (1.27).*

Figure 1.A.2: *The process and result of tail fitting the α_j spectra of QP solutions to generate better seed values.*

In terms of these coefficients, the TTF source terms are given by

$$T_\ell = \frac{1}{2}\omega_\ell^2 X_{\ell\ell\ell\ell} + \frac{3}{2}Y_{\ell\ell\ell\ell} + 2\omega_\ell^4 W_{\ell\ell\ell\ell} + 2\omega_\ell^2 W^*_{\ell\ell\ell\ell} - \omega_\ell^2(A_{\ell\ell} + \omega_\ell^2 V_{\ell\ell}) \tag{1.35}$$

$$\begin{aligned} R_{i\ell} = {} & \frac{1}{2}\left(\frac{\omega_i^2 + \omega_\ell^2}{\omega_\ell^2 - \omega_i^2}\right)(\omega_\ell^2 X_{i\ell\ell i} - \omega_i^2 X_{\ell i i\ell}) + 2\left(\frac{\omega_\ell^2 Y_{i\ell i\ell} - \omega_i^2 Y_{\ell i\ell i}}{\omega_\ell^2 - \omega_i^2}\right) \\ & + \left(\frac{\omega_i^2\omega_\ell^2}{\omega_\ell^2 - \omega_i^2}\right)(X_{i\ell\ell i} - X_{\ell i\ell i}) + \frac{1}{2}(Y_{ii\ell\ell} + Y_{\ell\ell ii}) + \omega_i^2\omega_\ell^2(W_{\ell\ell ii} + W_{ii\ell\ell}) \\ & + \omega_i^2 W^*_{\ell\ell ii} + \omega_\ell^2 W^*_{ii\ell\ell} - \omega_\ell^2(A_{ii} + \omega_i^2 V_{ii}) \end{aligned} \tag{1.36}$$

$$\begin{aligned} S_{ijk\ell} = {} & -\frac{1}{4}\left(\frac{1}{\omega_i + \omega_j} + \frac{1}{\omega_i - \omega_k} + \frac{1}{\omega_j - \omega_k}\right)(\omega_i\omega_j\omega_k X_{\ell ijk} - \omega_\ell Y_{i\ell jk}) \\ & - \frac{1}{4}\left(\frac{1}{\omega_i + \omega_j} + \frac{1}{\omega_i - \omega_k} - \frac{1}{\omega_j - \omega_k}\right)(\omega_j\omega_k\omega_\ell X_{ijk\ell} - \omega_i Y_{jik\ell}) \\ & - \frac{1}{4}\left(\frac{1}{\omega_i + \omega_j} - \frac{1}{\omega_i - \omega_k} + \frac{1}{\omega_j - \omega_k}\right)(\omega_i\omega_k\omega_\ell X_{jik\ell} - \omega_j Y_{ijk\ell}) \\ & - \frac{1}{4}\left(\frac{1}{\omega_i + \omega_j} - \frac{1}{\omega_i - \omega_k} - \frac{1}{\omega_j - \omega_k}\right)(\omega_i\omega_j\omega_\ell X_{kij\ell} - \omega_k Y_{ikj\ell})\,. \end{aligned} \tag{1.37}$$

1.C Frequency of Solution Checking

The frequency of applying the nonlinear solver to project back down to the QP solution plane is an important part of ensuring that the perturbative method remains applicable. If QP solutions are perturbed by too large an energy, or for too many iterations, the intermediate solutions may not be close enough to the solution plane to provide an adequate seed value. Such was the concern when examining the purported high-temperature solutions from existing sources.

For example, consider the process of applying perturbations of $\delta E = 0.01\%$ up to some intermediate temperature without projecting back to the QP plane, then projecting back every 100 iterations until a maximum temperature is reached. Starting with the QP solution corresponding to $\alpha_1 = 0.2$, the lower panel of figure 1.C.1 shows the result of repeated perturbations of $\delta E = 0.01\%$ that are not projected back the to QP plane.

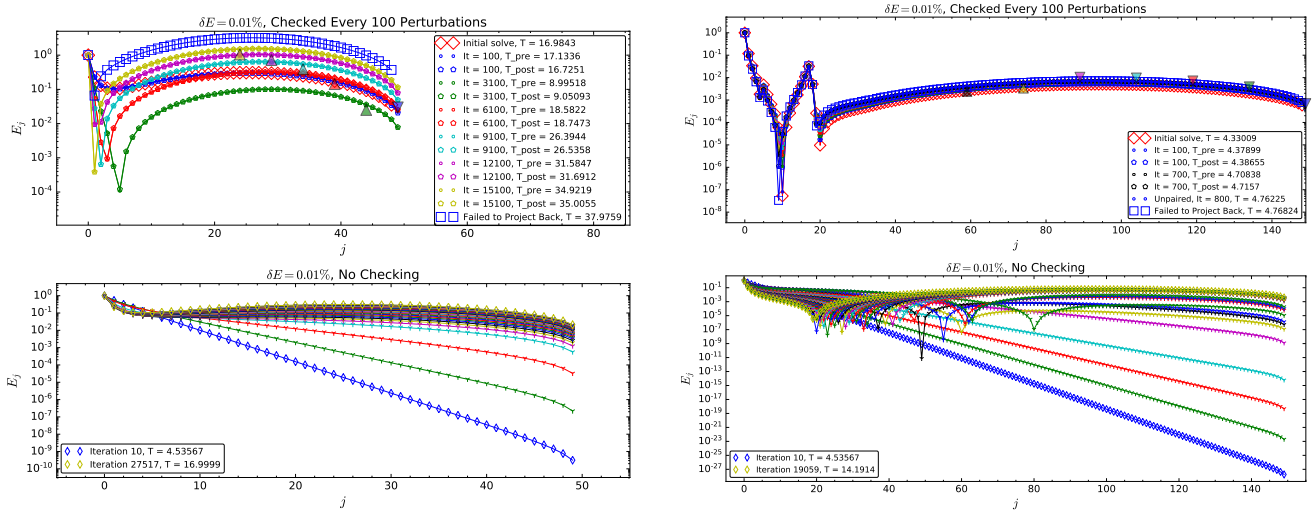

Figure 1.C.1: *Left: the result of unchecked perturbations of a $j_{max} = 50$ QP solution up to an intermediate temperature before switching to regular checking. Right: the same procedure is applied to a $j_{max} = 150$ QP solution.*

The behaviour of the spectra differ for the low and high j_{max} cases. For the $j_{max} = 50$ solutions, the

spectra in the lower panel of the figure can be remain smooth through more than 27,000 iterations of δE perturbations. When a temperature of approximately 17 is reached, the spectrum is used as a seed value for the nonlinear solver and a smooth solution is found. Continuing with the same δE, but reapplying the nonlinear solver produces mixed results; the temperatures of increasing iterations do not increase monotonically, but do always project back to a solution with nearly the same temperature. However, the spectra themselves are no longer C^1 differentiable by iteration 3,100. As discussed in § **??**, loss of differentiability is merely indicative of a change of sign in the alpha values; however, this is also accompanies a breakdown of the perturbative conditions in §1.4.2. Because only a small number of modes are considered, numerical solutions are still found by the Newton-Raphson solver but no longer represent physical states. Continuing this procedure, we find that the solver fails to find a solution even at the modest temperature of $T \simeq 38$.

The behaviour of the $j_{max} = 150$ solutions is consistent with their lower-mode number counterparts, albeit more pronounced. We see that kinks in the spectrum develop even when the nonlinear solver has not been applied. The intermediate solution used as a seed for the nonlinear solver did not project back to a nearby temperature, instead falling from $T \simeq 14.2$ to $T \simeq 4.3$. As the perturbative procedure continued, projection back to the QP plane was only possible in for a short time before no solutions could be found. We conclude that physically relevant solutions are restricted to values much closer to T_{th} than previously thought.